Downloaded from orbit.dtu.dk on: May 05, 2023

DTU Library

GPC light shaping a supercontinuum source

Kopylov, Oleksii; Bañas, Andrew Rafael; Villangca, Mark Jayson; Palima, Darwin; Glückstad, Jesper

Published in:
Optics Express

Link to article, DOI:
10.1364/OE.23.00184

Publication date:
2015

Document Version
Publisher's PDF, also known as Version of record

Link back to DTU Orbit

Citation (APA):
Kopylov, O., Bañas, A. R., Villangca, M. J., Palima, D., & Glückstad, J. (2015). GPC light shaping a supercontinuum source. *Optics Express*, *23*(3), 1894-1905. https://doi.org/10.1364/OE.23.00184

General rights
Copyright and moral rights for the publications made accessible in the public portal are retained by the authors and/or other copyright owners and it is a condition of accessing publications that users recognise and abide by the legal requirements associated with these rights.

- Users may download and print one copy of any publication from the public portal for the purpose of private study or research.
- You may not further distribute the material or use it for any profit-making activity or commercial gain
- You may freely distribute the URL identifying the publication in the public portal

If you believe that this document breaches copyright please contact us providing details, and we will remove access to the work immediately and investigate your claim.

GPC light shaping a supercontinuum source

Oleksii Kopylov, Andrew Bañas, Mark Villangca, Darwin Palima, and Jesper Glückstad*

DTU Fotonik,Dept. Photonics Engineering, Ørsted Plads 343 Technical University of Denmark, DK-2800 Kgs. Lyngby, Denmark

**jesper.gluckstad@fotonik.dtu.dk*

http://www.ppo.dk

Abstract: Generalized Phase Contrast (GPC) is a versatile tool for efficiently rerouting and managing photon energy into speckle-free contiguous spatial light distributions. We have previously shown theoretically and numerically that a GPC Light Shaper shows robustness to shift in wavelength and can maintain both projection length scale and high efficiency over a range $[0.75\lambda_0; 1.5\lambda_0]$ with λ_0 as the characteristic design wavelength. With this performance across multiple wavelengths and the recent availability of tabletop supercontinuum lasers, GPC light shaping opens the possibility for creatively incorporating various multi-wavelength approaches into spatially shaped excitations that can enable new broadband light applications. We verify this new approach using a supercontinuum light source, interfaced with a compact GPC light shaper. Our experiments give ~70% efficiency, ~3x intensity gain, and ~85% energy savings, limited, however, by the illumination equipment, but still in very good agreement with theoretical and numerical predictions.

©2015 Optical Society of America

OCIS codes: (070.6110) Spatial filtering; (070.0070) Fourier optics and signal processing; (120.5060) Phase modulation; (140.3300) Laser beam shaping.

References and links

1. A. E. Cerussi, D. Jakubowski, N. Shah, F. Bevilacqua, R. Lanning, A. J. Berger, D. Hsiang, J. Butler, R. F. Holcombe, and B. J. Tromberg, "Spectroscopy enhances the information content of optical mammography," J. Biomed. Opt. **7**(1), 60–71 (2002).
2. Y. Y. Cheng and J. C. Wyant, "Multiple-wavelength phase-shifting interferometry," Appl. Opt. **24**(6), 804 (1985).
3. E. L. Heffer and S. Fantini, "Quantitative oximetry of breast tumors: a near-infrared method that identifies two optimal wavelengths for each tumor," Appl. Opt. **41**(19), 3827–3839 (2002).
4. Y.-C. Chen, N. R. Raravikar, L. S. Schadler, P. M. Ajayan, Y.-P. Zhao, T.-M. Lu, G.-C. Wang, and X.-C. Zhang, "Ultrafast optical switching properties of single-wall carbon nanotube polymer composites at 1.55 μm," Appl. Phys. Lett. **81**(6), 975 (2002).
5. E. Papagiakoumou, "Optical developments for optogenetics," Biol. Cell **105**(10), 443–464 (2013).
6. E. Papagiakoumou, F. Anselmi, A. Bègue, V. de Sars, J. Glückstad, E. Y. Isacoff, and V. Emiliani, "Scanless two-photon excitation of channelrhodopsin-2," Nat. Methods **7**(10), 848–854 (2010).
7. D. Palima, C. A. Alonzo, P. J. Rodrigo, and J. Glückstad, "Generalized phase contrast matched to Gaussian illumination," Opt. Express **15**(19), 11971–11977 (2007).
8. S. Singh-Gasson, R. D. Green, Y. Yue, C. Nelson, F. Blattner, M. R. Sussman, and F. Cerrina, "Maskless fabrication of light-directed oligonucleotide microarrays using a digital micromirror array," Nat. Biotechnol. **17**(10), 974–978 (1999).
9. S. E. Chung, W. Park, H. Park, K. Yu, N. Park, and S. Kwon, "Optofluidic maskless lithography system for real-time synthesis of photopolymerized microstructures in microfluidic channels," Appl. Phys. Lett. **91**(4), 041106 (2007).
10. T. R. M. Sales, R. P. C. Photonics, C. Road, and R. Ny, "Structured Microlens Arrays for Beam Shaping," Proc. SPIE **5175**, 109–120 (2003).
11. C. Kopp, L. Ravel, and P. Meyrueis, "Efficient beamshaper homogenizer design combining diffractive optical elements, microlens array and random phase plate," J. Opt. A, Pure Appl. Opt. **1**(3), 398–403 (1999).
12. J. A. Hoffnagle and C. M. Jefferson, "Design and performance of a refractive optical system that converts a Gaussian to a flattop beam," Appl. Opt. **39**(30), 5488–5499 (2000).

#222075 - $15.00 USD Received 1 Sep 2014; revised 10 Dec 2014; accepted 12 Jan 2015; published 26 Jan 2015
(C) 2015 OSA

13. W. B. Veldkamp, "Laser beam profile shaping with interlaced binary diffraction gratings," Appl. Opt. **21**(17), 3209–3212 (1982).
14. M. R. Wang, "Analysis and optimization on single-zone binary flat-top beam shaper," Opt. Eng. **42**(11), 3106 (2003).
15. S. H. Lee and D. Grier, "Robustness of holographic optical traps against phase scaling errors," Opt. Express **13**(19), 7458–7465 (2005).
16. V. Arrizón, "Optimum on-axis computer-generated hologram encoded into low-resolution phase-modulation devices," Opt. Lett. **28**(24), 2521–2523 (2003).
17. J. Glückstad and D. Palima, *Generalized Phase Contrast: Applications in Optics and Photonic* (Springer, 2009).
18. J. Glückstad, L. Lading, H. Toyoda, and T. Hara, "Lossless light projection," Opt. Lett. **22**(18), 1373–1375 (1997).
19. P. J. Rodrigo, V. R. Daria, and J. Glückstad, "Real-time three-dimensional optical micromanipulation of multiple particles and living cells," Opt. Lett. **29**(19), 2270–2272 (2004).
20. A. Bañas, D. Palima, M. Villangca, T. Aabo, and J. Glückstad, "GPC light shaper for speckle-free one- and two-photon contiguous pattern excitation," Opt. Express **22**(5), 5299–5311 (2014).
21. A. Bañas, O. Kopylov, M. Villangca, D. Palima, and J. Glückstad, "GPC Light Shaper: static and dynamic experimental demonstrations," Opt. Express **22**(20), 23759–23769 (2014).
22. J. Glückstad and P. C. Mogensen, "Optimal phase contrast in common-path interferometry," Appl. Opt. **40**(2), 268–282 (2001).
23. C. A. Alonzo, P. J. Rodrigo, and J. Glückstad, "Photon-efficient grey-level image projection by the generalized phase contrast method," New J. Phys. **9**(5), 132 (2007).
24. D. Palima and J. Glückstad, "Multi-wavelength spatial light shaping using generalized phase contrast," Opt. Express **16**(2), 1331–1342 (2008).
25. J. Jahns, "All-reflective planar-integrated free-space micro-optical femtosecond pulse shaper," Opt. Eng. **48**(12), 123001 (2009).
26. V. Bagnoud and J. D. Zuegel, "Independent phase and amplitude control of a laser beam by use of a single-phase-only spatial light modulator," Opt. Lett. **29**(3), 295–297 (2004).
27. J. Liang, R. N. Kohn, Jr., M. F. Becker, D. J. Heinzen, M. R. Douglass, and P. I. Oden, "High-precision beam shaper for coherent and incoherent light using a DLP spatial light modulator," in *Proceedings of SPIE - the International Society for Optical Engineering*, M. R. Douglass and P. I. Oden, eds. (2011), **Vol. 7932**, pp. 793208.
28. J. Glückstad, D. Palima, P. J. Rodrigo, and C. A. Alonzo, "Laser projection using generalized phase contrast," Opt. Lett. **32**(22), 3281–3283 (2007).
29. V. Daria, J. Glückstad, P. C. Mogensen, R. L. Eriksen, and S. Sinzinger, "Implementing the generalized phase-contrast method in a planar-integrated micro-optics platform," Opt. Lett. **27**(11), 945–947 (2002).

1. Introduction

1.1 Multi-wavelength light shaping

Many important applications of the interaction of light with matter strongly depend on the illumination wavelength. On a fundamental level, the way electrons move between atomic energy levels depend on the interacting photons' energy, which in turn can be controlled by a proper choice of wavelength. Hence, for such studies, a laser source containing multiple wavelengths is much more versatile than normal monochromatic lasers. Tabletop supercontinuum light sources have thus been used in a plurality of applications that include optical coherence tomography, spectroscopy, optical characterization or sensing, imaging and microscopy, neuroscience and neurophotonics, metrology among many others.

Multi-wavelength techniques are invaluable in spectroscopy [1] and provide beneficial enhancements in interferometry [2], well-established fields with significance that cannot be overemphasized. Exploiting the wavelength-dependent material response also allows for controlled photo-excitation, targeted monitoring [3], and even simultaneous excitation and monitoring in pump-probe geometries [4].

Light shaping, on the other hand, increases the diversity of such applications by adding spatial control or selectivity to such light-matter interactions. For example, in two-photon optogenetics research [5], one would like to selectively illuminate intricate patterns of dendrites or axons within neurons [6]. As laser sources typically have limited shapes, many light shaping approaches have been studied to address different demands such as efficiency, speed, beam quality or economy concerns. A typical light source would have a TEM_{00} or Gaussian profile. Using an amplitude modulation by placing a shaped aperture on the path of

#222075 - $15.00 USD Received 1 Sep 2014; revised 10 Dec 2014; accepted 12 Jan 2015; published 26 Jan 2015
(C) 2015 OSA

the beam is inefficient. Around 70%, or even more if a more uniform intensity output of the incident power is needed, can be lost while illuminating a rectangle with an expanded Gaussian beam [7]. Besides the obvious disadvantages of inefficiency, the high price tag of state-of-the-art laser sources demands an economical way of managing their available photons. With supercontinuum laser sources, it also becomes important to shape light with consistent output dimensions and efficiency across different wavelengths.

1.2. Photon efficient light shaping

Amplitude masks are straightforward, robust to wavelength change, and are dynamically reconfigurable using spatial light modulators (SLM) as commonly found in consumer display projectors [8,9]. However, as mentioned, the energy inefficiency of amplitude masking is low. Hence, a number of solutions based on non-absorbing or phase-only methods exist for the efficient transformation of a Gaussian beams into user specified patterns. Static beam shapers such as engineered diffusers, microlens arrays or homogenizers [10,11] are robust to wavelength shifts but suffer from speckled or grainy output intensities. Refractive mapping [12] does not suffer from grainy or specked output, but its use of specially optimized aspheric lenses, makes it hard to adapt to different shapes. Diffractive approaches such as computer generated holography, diffractive optical elements or phase plates [13,14] form the image at the far field or at a Fourier plane, resulting to output that scales with wavelength. Although SLM based dynamic holograms matched to individual wavelengths may be superimposed into a single element [15], hologram crosstalk generates noise from the mismatched wavelengths. Furthermore, iteratively designed diffractive approaches are more prone to convolution effects that blur the edges of the shaped output and considerably fluctuate due to speckles in the intensity distribution. Diffractive optics encoding complex amplitudes avoid speckles but, nonetheless, yield lower efficiencies (e.g., 49.2% efficiency was reported in [16].

1.3. Generalized phase contrast

The Generalized Phase Contrast method (GPC) [17] is a versatile technique for generating patterned illumination. By projecting intensity images that visualize phase inputs, the GPC is a fairly straightforward technique with a high light utilization [18]. It can generate a wide variety of patterns [7,19–21] and accommodates various illumination profiles [7,22,23]. With reconfigurable phase inputs from phase-only SLMs, it is an effective laser projection system for dynamic multiple beam optical trapping [19]. Furthermore, unlike other phase-only beam shaping techniques mentioned, GPC works on a 4*f* imaging geometry, hence avoiding wavelength dependent scaling of the output which makes it a good candidate for shaping composite multi-wavelength or supercontinuum lasers [24]. The 4*f* geometry can accommodate different filters in the Fourier plane and different 4*f* beam shaping systems have also been proposed by others [25–27]. Among these, GPC is unique in shaping light using a direct phase to intensity mapping.

In GPC, a phase-only aperture directly representing the desired output intensity is imaged through its interference with a synthetic reference wave (SRW). This common path mapping configuration renders steep well-defined edges in the shaped intensity output. The SRW is formed by phase shifting the lower spatial frequencies through a phase contrast filter (PCF) at the Fourier plane (Fig. 1). GPC could thus be implemented with binary phase plates that are easier to mass-produce with standard cleanroom or foundry processes common for silicon devices or micro-electronics. Phase masks and PCFs can also be implemented in a number of alternative ways such as a hole in a piece of glass with a controlled thickness or as a bump or depression on a reflective surface. Techniques used for single mode fibers can also be adopted if dealing with high power lasers. Furthermore, the target output shapes could easily be replaced without increasing the fabrication cost or complexity. Light patterns formed with GPC can reach efficiencies of up to 84% in contrast to simple techniques such as rectangular

#222075 - $15.00 USD Received 1 Sep 2014; revised 10 Dec 2014; accepted 12 Jan 2015; published 26 Jan 2015
(C) 2015 OSA

irises [20]. Moreover, the average light intensity in the patterned region is ~3 times larger than the average intensity within the corresponding region of the incident Gaussian.

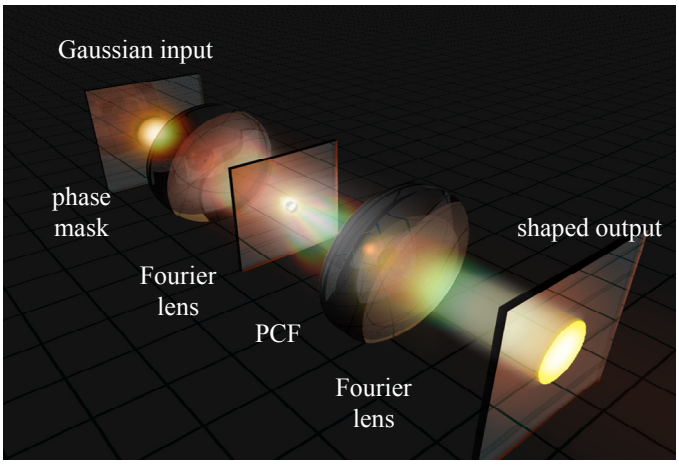

Fig. 1. Supercontinuum light shaping with the GPC Light Shaper. In addition to a standard imaging or telescopic setup formed by the two Fourier lenses, GPC uses a simple binary phase mask at the input and a phase contrast filter at the Fourier plane. In this illustration a Gaussian beam is efficiently transformed into a tophat without speckles.

In this work, we experimentally demonstrate that a GPC-based light shaper works with multi-wavelength Gaussian illumination as predicted in [24]. We briefly review the optimization of a GPC Light Shaper (LS) system in section 2 and also consider the physical effects of changing the illumination wavelength. Sections 3 and 4 present experiments that illustrate GPC LS across multiple wavelengths and discuss the results. Finally, section 5 presents the conclusions and outlook.

2. Background

2.1. Reshaping Gaussian beams with GPC

To have a successfully working GPC system, one has to first determine parameters of a phase mask and PCF given the expected wavelength, beam diameter and other constraints. We therefore summarize how to choose optimal phase masks and PCF sizes based on the formulations in [20] – all currently based on π-shifting phase values at the design wavelength. Given a Gaussian beam with a $1/e^2$ radius, w_0, illuminating a phase mask with phase profile $\phi(x,y)$, we define its normalized Fourier zero order, $\bar{\alpha}$, as

$$\bar{\alpha} = \frac{1}{\pi w_0^2} \iint \exp\left[-\left(x^2+y^2\right)/w_0^2\right] \exp\left[i\phi(x,y)\right] dxdy. \tag{1}$$

In the absence of an input phase mask, the input Gaussian would be focused into another Gaussian at the Fourier plane. Assuming a wavelength, λ_0, and focal length, f, the Gaussian waist radius at the Fourier plane, w_f, is given by

$$w_f = \lambda_0 f / (\pi w_0). \tag{2}$$

Δr_f is the phase contrast filter's π-shifting region's radius and is measured relative to this Fourier transformed Gaussian. It is characterized by the dimensionless η given by

$$\eta = \Delta r_f / w_f \tag{3}$$

#222075 - $15.00 USD Received 1 Sep 2014; revised 10 Dec 2014; accepted 12 Jan 2015; published 26 Jan 2015
(C) 2015 OSA

By imposing amplitude matching with a synthetic reference wave [7], and that Δr_f coincides with the Fourier distribution's first zero crossing (first dark ring) [20], the conditions for optimal contrast and efficiency of the GPC output lead to the following equations

$$\eta = \sqrt{-\ln\left(1-\sqrt{1/2}\right)} = 1.1081, \tag{4}$$

$$\overline{\alpha} = \sqrt{1/2} = 0.7071. \tag{5}$$

Equations (4) and (5) summarize the conditions for an optimally performing GPC system under Gaussian illumination. The fixed value for η in Eq. (4) means that a reconfigurable GPC system with a fixed PCF will consistently perform optimally with different phase masks satisfying Eq. (5). The phase mask's geometry, $\phi(x,y)$, should thus be tweaked such that Eq. (5) is satisfied. For simple shapes such as a circle and a rectangle, we have analytically shown how to scale $\phi(x,y)$ [20]. We show how these conditions are used for fabricating static glass filters in section 4.

2.2. The effects of changing the illumination wavelength

The output of a GPC LS is typically represented as:

$$o(x,y) = a(x,y) + \left(\exp(i\theta)-1\right)\Im^{-1}\left\{\mathrm{circ}\left(\frac{\sqrt{f_x^2+f_y^2}}{\eta w_f}\right)A\left(f_x,f_y\right)\right\} \tag{6}$$

where $a(x,y) = a_0(x,y)\exp(\mathrm{i}\,\phi(x,y))$ is the image of the phase modulated Gaussian input. Equation (6) shows the output as the superposition of the input's image, $a(x,y)$, with a synthetic reference wave (SRW) whose spatial variation, $\Im^{-1}\{\ldots\}$, is the low-pass filtered input– $\Im^{-1}\{\ldots\}$ transforms back to real space the filtered frequencies resulting from the multiplication of the Fourier transform of the input, $A(f_x,f_y)$, with the truncating circular aperture, circ(…), which has the size of the PCF's phase-shifting region. The SRW is further multiplied by a complex scaling factor that depends on the PCF phase shift, θ. When the optimal GPC parameters for a particular wavelength of Gaussian illumination are found, it would be straightforward to numerically evaluate its performance across different wavelengths. However, an understanding of the underlying physics can give useful insights, as we briefly outline below.

For a given wavelength, the output in Eq. (6) yields optimal efficiency when using π-phase-shifts for the input and filter masks [20]. Therefore, at first glance, the range of wavelengths from a supercontinuum light sources would seem problematic for the GPC LS. Phase masks that have been etched to a depth, d_0, to produce π- phase shift at a given design wavelength, λ_0, will produce a different phase shift when illuminated by another wavelength λ. Etching the input and filter phase masks simultaneously on the same glass wafer results in a common phase shift given by

$$\phi(\lambda) = \theta(\lambda) = \frac{2\pi}{\lambda}\left(n_{air} - n_{\lambda,glass}\right)d_0 = \pi\frac{\lambda_0}{\lambda}\frac{\Delta n_\lambda}{\Delta n_{\lambda 0}} \tag{7}$$

where we also included material dispersion (primarily due to glass). Similarly, from Eq. (2) and (3) above, the dimensionless η will depend on wavelength as:

$$\eta = \frac{\Delta r_f \pi w_0}{\lambda f} = \frac{\lambda_0}{\lambda}\eta_0 \tag{8}$$

#222075 - $15.00 USD Received 1 Sep 2014; revised 10 Dec 2014; accepted 12 Jan 2015; published 26 Jan 2015
(C) 2015 OSA

where η_0 is the value of the parameter at the design wavelength, λ_0 (assuming the incident beam waist is independent of wavelength).

For simplicity, let us consider the case of Gaussian-to-tophat shaping. This requires an input phase mask having a circular phase shifting region of radius Δr. We may gain some insights about how shifting the wavelength would affect performance by looking at the on-axis value of the superposition:

$$o(0,0) = exp(i\phi) + \left[\exp(i\theta) - 1\right]\left\{1 - \exp\left(-\eta^2\right) + \eta^2\left[-1 + \exp(i\phi)\right]\left[1 - \exp\left(-\zeta^2\right)\right]\right\} \quad (9)$$

where $\zeta = \Delta r / w_0$ is a dimensionless parameter describing the size of the input phase mask radius relative to the input Gaussian waist, and therefore, the size of the output tophat relative to the Gaussian waist that can be imaged at the output by the 2 lenses. The field around the phase-shifting region of the PCF is very well approximated by a displaced Gaussian [20], and so we used this to find the on-axis value of the low-pass filtered input. Using the known wavelength dependence of the phase shifts (θ, ϕ) and the parameter η, we can determine how the intensity will change with wavelength. Figure 2(a) shows how the on-axis intensity is affected when sweeping the wavelength from 350 to 750nm when using GPC parameters optimized for λ_0 = 532nm (the simulations used η = 1.1081and ζ = 0.3979 according to the optimization procedure described in [20] and applied the dispersion properties of fused silica). For comparison, the graph also plots the wavelength dependence for a suboptimal case that uses a smaller input filter, ζ = 0.3 that corresponds to a smaller tophat output. The resulting upper trace in Fig. 2(a) shows that this smaller tophat exhibits a higher peak intensity but a more pronounced wavelength dependence relative to the optimized case (the lower trace in Fig. 2(a) is flatter). Moreover, when comparing conversion efficiencies using the power within the shaped area (Intensity × Area), it is the bigger tophat, ζ = 0.3979, obtained by the optimization procedure obtained in [20] that yields a higher efficiency (see efficiency comparisons in [20]). This means that the higher intensity within the smaller tophat, ζ = 0.3, is unable to compensate for its smaller area resulting in lower efficiency

To visualize how GPC's robustness to wavelength changes arises, we plotted how the on-axis image, exp(iϕ), and the SRWs corresponding to the two tophats, ζ = 0.3 and ζ = 0.3979, drift in the complex plane as the input wavelength changes from 380nm (A,D) to 700nm (C,F) for phase masks designed for 532nm (B,E). Illustrative phasor diagrams of the superposition are shown for selected wavelengths (A–F). The phasor diagrams show optimal superposition at the design wavelength and, as expected, the input phase deviates a lot from π over the chosen wavelength range. However, unlike the input phase, the SRW phase remains close to π over the range of wavelengths. When using non-π-phase modulated input, optimizing GPC requires finding an appropriate non-π-phase-shifting PCF that will create an SRW that is π-out-of-phase with the designated dark regions to minimize losses by ensuring optimum destructive interference [28]. In this case, we can see that the SRW is able to be close to π-out-of-phase with the 0-phase encoded background. This indicates that the corresponding non-π-phase shift of the PCF due to the change in wavelength ends close to the optimal phase shift. In effect, the input phase changes are compensated by the corresponding PCF phase change when shifting the wavelength away from the design wavelength. This compensation is explained in more detail in [24].

#222075 - $15.00 USD Received 1 Sep 2014; revised 10 Dec 2014; accepted 12 Jan 2015; published 26 Jan 2015
(C) 2015 OSA

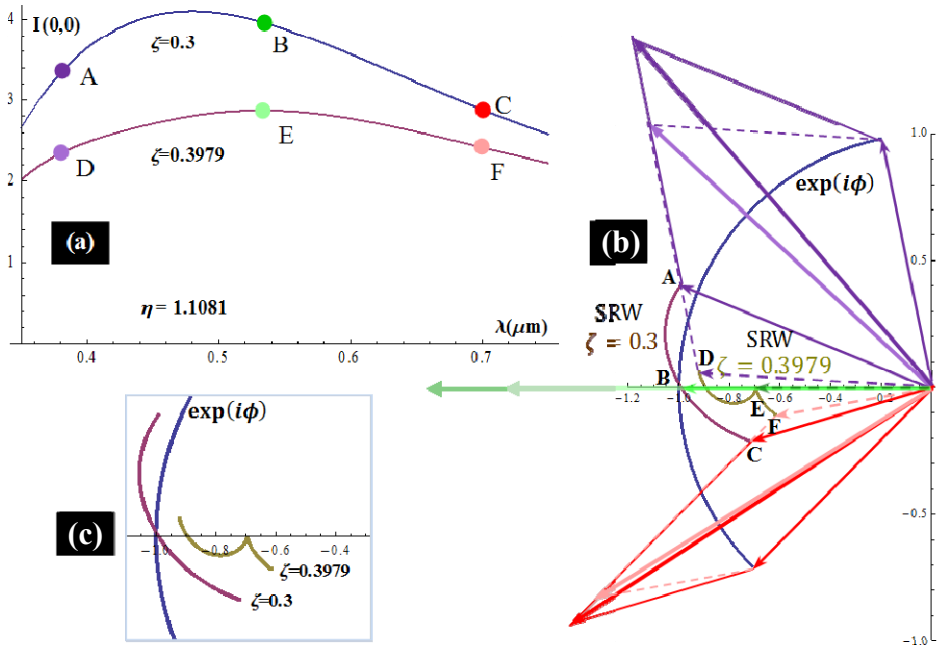

Fig. 2. Wavelength dependence using GPC parameters optimized for Gaussian-to-tophat shaping at $\lambda_0 = 532$nm. (a) On-axis intensity vs wavelength shows that the efficiency optimized tophat size ($\zeta = 0.3979$) exhibits a flatter wavelength response than a smaller tophat ($\zeta = 0.3$). (b) Complex plane visualization illustrating how the phasors drift from as the wavelength changes. Phasor diagrams illustrate the on-axis output superposition [cf Eq. (6)] of the modulated Gaussian, exp(iϕ), with the corresponding SRW phasors for the two tophats, marked $\zeta = 0.3$ and $\zeta = 0.3979$, at selected wavelengths marked A–C (D–F) in (a). (c) Zoom-in of how the SRW phasors drift as the wavelength changes from A–C (D to F) for $\zeta = 0.3$ ($\zeta = 0.3979$).

3. Light shaping experiments

3.1. Construction of a pen sized GPC LS

The GPC LS used for our static experiments was designed to interface directly with the output of laser sources in free space. Commercial lasers typically have beam diameters of around 1mm to 5mm. Using two f = 50mm Fourier lenses allowed us to keep the setup compact. This also allows cheap yet controlled mask fabrications with wet etching and off-the-shelf optics assembly. The GPC LS assembled with half-inch optics and 16mm cage system from Thorlabs is shown in Fig. 3. Its overall length is a little over $3f$ = 150mm, which is around the size of a usual pen. For more compact implementations, such as for OEM use, integrated micro-optics platforms [29] or alternative fabrication and assembly techniques can also be adopted. When compactness is not a requirement, longer focal lengths can be used to minimize the focused light-intensity at the PCF.

#222075 - $15.00 USD Received 1 Sep 2014; revised 10 Dec 2014; accepted 12 Jan 2015; published 26 Jan 2015
(C) 2015 OSA

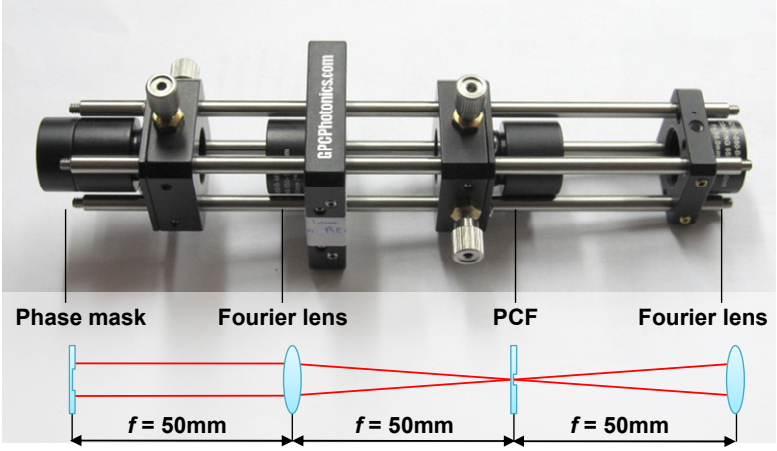

Fig. 3. Pen-sized GPC Light Shaper using two f = 50mm Fourier lenses and half inch optics assembly.

3.2. PCF and phase mask preparation

We designed the GPC LS for use with the following parameters: laser beam waist diameter $2w_0$ = 1mm, laser wavelength λ_0 = 532nm and focal length of lenses as f = 50mm. The material used for the phase mask and PCF is fused silica (n = 1.46 at λ = 532nm). The PCF radius is calculated using Eqs. (3)-(4), hence,

$$\Delta r_f = \eta \frac{\lambda_0 f}{\pi w_0} = \frac{1.1081 \times 0.532\mu\text{m} \times 50\text{mm}}{\pi \times 0.5\text{mm}} = 18.77\mu\text{m} \tag{10}$$

The phase masks were based on simple shapes (circle, square, and rectangle) and arbitrary bitmap images (e.g. globe, logos) that were scaled with respect to the preferred beam diameter such that Eq. (5) is satisfied. Conventional UV-lithography technique followed by wet etching in the buffered HF (BHF) was used to form the patterns. The etch depth was determined such that it gives a half wavelength optical path difference relative to the un-etched surroundings:

$$\text{etch depth} = (\lambda_0 / 2)/(n-1), \tag{11}$$

where n is the refractive index of fused silica.

Hence, the etch depth used is ~577nm. This wavelength was chosen as a central wavelength for the visible part of the spectrum of the supercontinuum laser we used and to work with widely used green (532nm) lasers. From a four-inch wafer, the phase masks and PCFs were diced such that they can be fitted into half-inch optics mounts.

3.3. Optical setup

The setup used for the testing a GPC LS across different wavelengths is shown in Fig. 4. The interchangeable phase masks were used to form a variety of speckle-free contiguous patterns at selected wavelengths.

#222075 - $15.00 USD Received 1 Sep 2014; revised 10 Dec 2014; accepted 12 Jan 2015; published 26 Jan 2015
(C) 2015 OSA

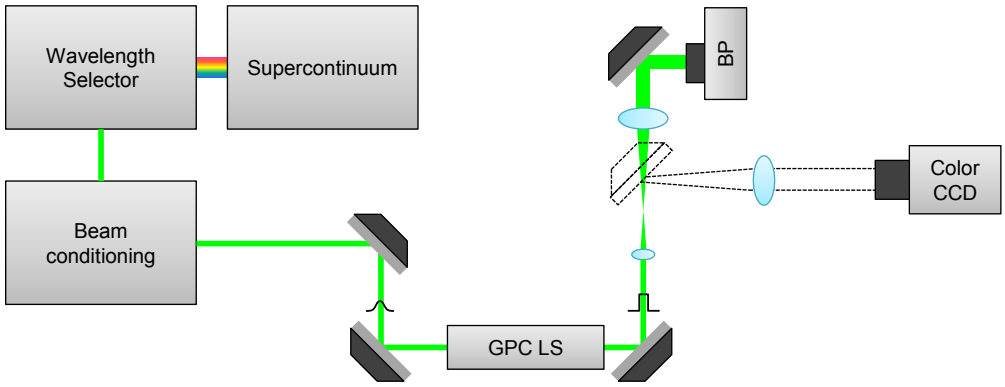

Fig. 4. GPC Light Shaper setup using a multi-wavelength illumination. The GPC Light Shaper (GPC LS) is illuminated with $2w_0$ = 1mm. The light is passed through a GPC system and then imaged onto a color CCD camera or a beam profiler (BP).

For our light source, we used a supercontinuum laser from NKT Photonics (SuperK Koheras) that has a 1mm beam diameter. The beam is guided through the wavelength selector (SuperK Select from NKT Photonics). Light collimation and guidance after the wavelength selector was performed using fiber delivery system (SuperK Connect from NKT Photonics). It should be mentioned that the fiber output beam diameter was slightly wavelength dependent. The beam diameter was close to 1mm at 532nm and increases with wavelength. The spectral FWHM of the filtered beam was 1.5-4 nm depending on the wavelength. The light was then directed to the GPC LS using relay mirrors that also provided beam alignment. Output from the GPC LS was magnified (2x) then guided either to a beam profiler (Gentec-EO) or to a color CCD. The beam profiler's linear intensity response allows post-analysis while the color CCD better visualizes the multi-wavelength results.

4. Light shaping results

4.1 Results using laser-line bandpass filters

For initial testing, we first assessed the light shaper's performance on its design wavelength – 532nm – by placing a 532nm laser-line band-pass filter along the SuperK path. Figure 5 presents different GPC output shapes tested by interchanging the phase masks on the same GPC LS. To rule out reflection losses, the Gaussian reference is obtained when the PCF is misaligned and the beam goes through the same components. However, to prevent edge effects from the etched pattern, the phase mask was completely removed from the GPC LS. Hence, the reference Gaussian is marginally more intense and the reported efficiencies are marginally lower.

We characterized the following: efficiencies, gain and energy savings. Efficiency is measured as the ratio between the power within the output shape and power in the reference Gaussian. Gain compares the (averaged) peak intensities of the output shape and reference Gaussian. Energy savings takes efficiency and gain into account as it quantifies how much energy would have been lost if using a less efficient amplitude masking system using more power (i.e. the ~3x gain) to get similar results to that from a GPC LS [20]. For rather complicated speckle-free high contrast structures, presented in Fig. 5, the efficiencies, gain, and energy savings are ~80%, ~3x and ~90%, respectively. The GPC LS allows not only to precisely shape the laser beam but also to increase light intensity in the pattern region to ~3 times. This gain is clearly depicted by comparing Fig. 5(a) showing, the reference Gaussian to the GPC generated output Fig. 5 (b)-5(e) using the same input laser power.

#222075 - $15.00 USD Received 1 Sep 2014; revised 10 Dec 2014; accepted 12 Jan 2015; published 26 Jan 2015
(C) 2015 OSA

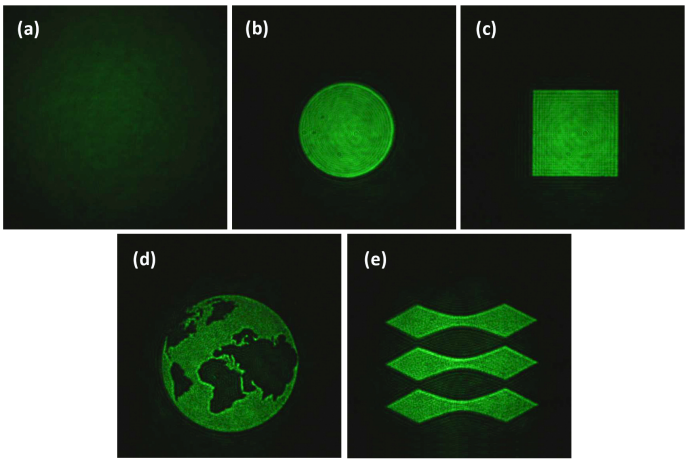

Fig. 5. CCD images of the green laser light intensity without a phase mask (a), and with the circle (b), square (c), globe (d), and DTU logo (e) phase masks, respectively.The input laser power is kept the same for all cases.

4.2 Results using the wavelength selector

Having confirmed results for the 532nm design wavelength, the GPC LS was then tested with multiple wavelengths from the wavelength selector. As noted, the output beam size was wavelength-dependent and slightly differs from 1mm - output beam diameter of the SuperK without the wavelength selector - which was used in the GPC LS design. This influences measurements making efficiencies lower than expected. However, the overall performance is still within acceptable experimental variations, indicating the tolerance of the GPC LS.

Figure 6(a)-6(f) presents a globe pattern obtained at different wavelengths. The SuperK power was adjusted for different wavelengths to maintain fairly uniform image brightness on the CCD captures. Even though wavelength was being changed over a wide range, the final patterns shows high contrast and brightness uniformity.

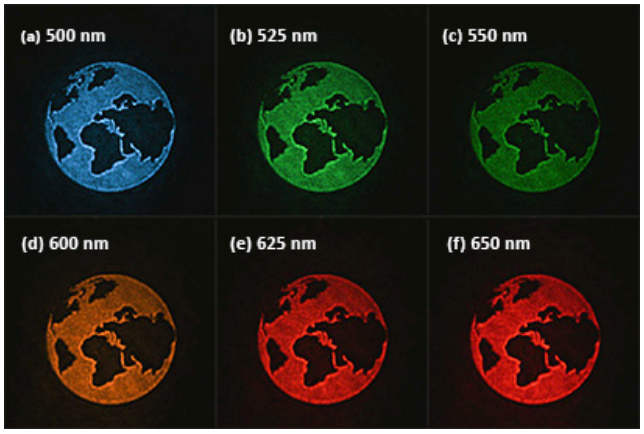

Fig. 6. Color CCD images of GPC projections from the same setup, as the wavelength selector is varied from 500nm to 650nm (a)-(f) (see Media 1).The power at different wavelengths is adjusted individually for visibility.

To confirm previous theoretical and numerical predictions [24], we measured the dependence of the GPC LS's efficiency against different wavelengths. The measurements were performed at 25nm steps, changing the tested wavelength and maintaining a small FWHM. Figure 7 shows the experimental data. The error bars for the experimental data were

#222075 - $15.00 USD Received 1 Sep 2014; revised 10 Dec 2014; accepted 12 Jan 2015; published 26 Jan 2015
(C) 2015 OSA

obtained from the difference between several measurements performed at the same wavelength (five in average).These error bars allow room for slight fluctuations caused by the laser beam's intensity and beam size.

The acquired efficiencies and energy savings are, as expected, marginally lower than the simulated ones [24]. The main reason was the deviations from the beam diameter that the GPC LS was designed for. Experiments with the beam obtained directly from the green-filtered SuperK (Fig. 5) has shown better results closer to theoretical predictions. Despite being lower than theoretical predictions, the GPC LS exhibited good beam shaping performance across the whole visible range with slightly lower results in the very red spectrum range, also as simulations predicted [24]. It should also be noted that as the phase mask was removed to obtain a clean Gaussian signal, partial reflections that the phase mask introduces were also withdrawn. Therefore, the real efficiency is somewhat higher than what we have measured.

The gain was maintained at the level of ~3x throughout the wavelength range. The relative incrase in gain level, seen at the red range (i.e. from 650nm to 675nm), can be explained by the slightly larger beam diameter that causes a mismatch of the SRW. This is also consistent with the lowered efficiencies as the SRW mismatch lessens the effect of destructive interferene that supposedly defines the dark background. The counteracting effects of gain and efficiency, however, effectively maintains a fairly high energy savings value.

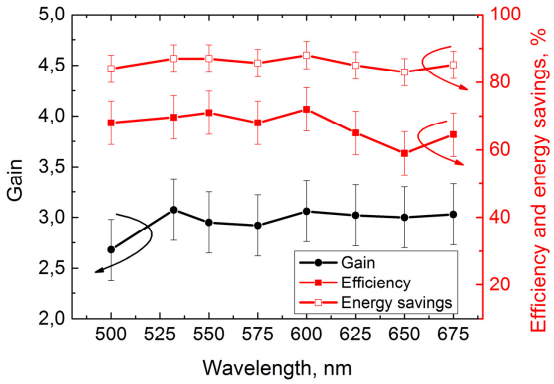

Fig. 7. Wavelength dependence of the efficiency, energy savings and gain of a GPC Light Shaper illuminated with a Gaussian beam. The GPC LS is designed for 532 nm and used a circular phase mask.

5. Summary and outlook

We have experimentally shown that light shaping based on the Generalized Phase Contrast method shows robustness to wavelength change. The GPC-based projections maintain high quality and efficiency over a doubling of wavelength in Gaussian beam shaping. With some wavelength dependent deviations, experiments showed around ~70% efficiency, ~3x intensity gain and ~85% energy savings compared to the commonly implemented hard-truncated expanded Gaussian. The energy saved by using a GPC LS makes it attractive for many applications wherein light is best utilized in a particular shape, e.g. rectangles for spatial light modulator illumination or digital display projection, circles for laser materials processing or even intricate biological patterns found in neurophotonics research if coupled with a dynamic broadband spatial light modulator. Furthermore, the added benefit of broadband light shaping, makes it an attractive enabling tool for advanced biological research. For even better performance of the GPC LS, i.e. higher efficiency, broadband anti-reflection coating on top of both the phase mask and the PCF can be considered.

#222075 - $15.00 USD Received 1 Sep 2014; revised 10 Dec 2014; accepted 12 Jan 2015; published 26 Jan 2015
(C) 2015 OSA

Acknowledgments

We would like to thank the following for financial support, the Copenhagen Cleantech Cluster (CCC) for GAP funding, the DTU PoC-Board for Proof-of-Concept funding and the Enhanced Spatial Light Control in Advanced Optical Fibers (e-space) project by the Danish Council for Strategic Research. We also thank NKT Photonics A/S for lending us the supercontinuum laser (SuperK Koheras) and the wavelength selector (SuperK Select) with the fiber delivery system (SuperK Connect).

#222075 - $15.00 USD Received 1 Sep 2014; revised 10 Dec 2014; accepted 12 Jan 2015; published 26 Jan 2015
(C) 2015 OSA